TRANSITION JUMP SYSTEM FOR THE FERMILAB BOOSTER

W. Merz, C. Ankenbrandt, and K. Koepke
Fermi National Accelerator Laboratory
Batavia, Il 60510

Summary

A transition-jump system recently installed in the Fermilab Booster is described. Early results of the commissioning are presented.

Introduction

For proton accelerators in which the transition energy lies within the operating energy range, some growth of the longitudinal emittance generally occurs as the beam passes through the transition energy. The amount of growth increases with beam intensity and constitutes a limiting factor on the attainable beam intensity and brightness. Microwave and/or negative-mass instabilities can cause longitudinal emittance growth near transition. Furthermore, space-charge effects create a difference in the effective longitudinal focusing force before and after transition, causing bunch-length oscillations which can filament, leading to dilution of the effective longitudinal emittance. All of these effects cause emittance growth in the Fermilab Booster at high intensity.

A transition-jump system can greatly reduce the deleterious effects of passing through transition at high intensity by reducing the time that the beam spends near the transition energy. For example, the CERN PS has profited from such a system for a long time [1]. Sorenssen [2] has reviewed the problems that occur at transition and the efficacy of various proposed solutions. The system described here, which was recently installed in the Fermilab Booster, is derived from a conceptual design by Teng [3]. Confidence that the system would ameliorate the Booster problems was reinforced by longitudinal tracking simulations performed by Lucas and MacLachlan [4].

Figure 1 illustrates the designed variation of the transition energy. It shows the time dependence of γ and of γ_t, the beam energy and the lattice transition energy in units of the proton rest energy. The γ_t of the normal lattice is of course constant at 5.446. The rate of change of γ when it crosses the normal transition energy is 0.406/msec. The transition jump system causes the indicated variation of γ_t. The initial rapid reduction of γ_t by as much as one unit occurs in about 0.1 msec, thereby increasing the rate of passage through transition by a factor of 25. The subsequent relaxation back to the normal value is

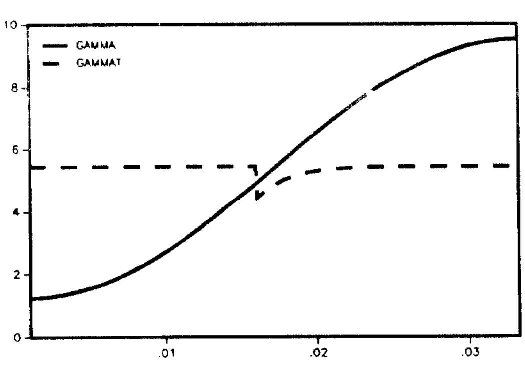

Figure 1. The time dependence of γ and γ_t.

*Operated by the Universities Research Association, Inc., under contract with the U.S. Dept. of Energy

roughly exponential with a time constant of about 2 msec so that, when the system is operating at full current, the initial rate of change of γ_t during the decay roughly matches the rate of change of γ.

Lattice Modifications

The normal Booster lattice consists of 24 identical periods, each containing 4 combined-function gradient magnets in a FOFDOOD configuration, where "O" designates a 1.2 meter short straight section and "OO" designates a 6.0 meter long straight section. The transition-jump system consists of 12 pulsed quadrupoles of alternating polarity, evenly spaced around the circumference in every other short straight section, between the focusing magnets of the regular lattice. The pulsed quadrupoles break the 24-fold symmetry of the regular lattice, creating a variation of the lattice functions with a sixfold periodicity. Teng [3] showed that a considerable change of the dispersion function (and with it γ_t) can be achieved with a relatively minor change of the amplitude functions β_x, β_y by perturbing the focusing at a harmonic close to the horizontal tune. In the present case, with a superperiodicity of six and a nominal horizontal tune of 6.7, γ_t is reduced; if the tune were lower than the periodicity of the perturbation, γ_t would be increased.

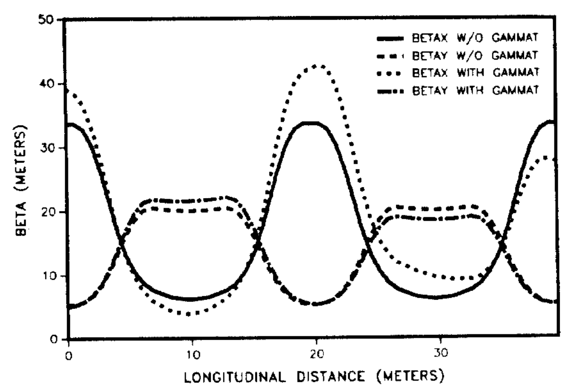

Figure 2. The betatron amplitude functions for the normal lattice and for $\Delta\gamma_t=-1$.

Figure 2 shows the calculated horizontal and vertical amplitude functions with the normal lattice and with the pulsed quadrupoles energized to change γ_t by one unit. The lattice functions are mirror-symmetric about the pulsed quadrupoles, so only half a superperiod (1/12th of the ring) is shown; a horizontally focusing pulsed quadrupole is at the left and a defocusing quadrupole is at the right edge of the figure. With equal-strength focusing and defocusing quadrupoles, the calculated change in the horizontal tune is +0.09 at full excitation; therefore, the ratio of quadrupole lengths was chosen to be F/D=15/17, limiting the magnitude of the horizontal tune variation to about 0.01. Measurements confirm the small predicted tune change.

Figure 3 shows the dispersion functions calculated by SYNCH for half a superperiod for three cases: $\Delta\gamma_t$=0,-0.323, and -1. The figure also shows measured values of the dispersion function for the second case; the agreement with the SYNCH calculation is good. To measure the dispersion, the closed orbit difference generated by changing the offset in the radial feedback loop was recorded, then averaged over

CH2387-9/87/0000-1343 $1.00 © IEEE
PAC 1987

the six superperiods. The momentum offset corresponding to a given radial offset was estimated by normalizing to the orbit shifts generated by the same radial offset with the normal lattice.

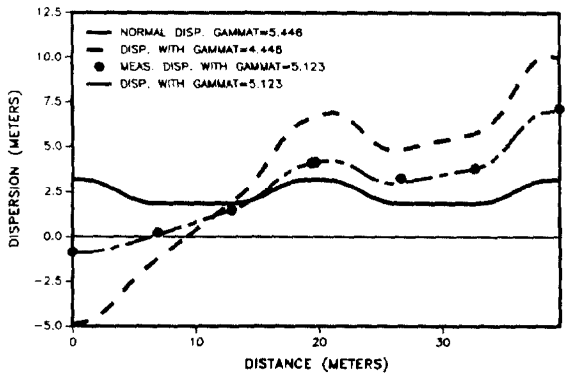

Figure 3. Calculated dispersion function for $\Delta\gamma_t=0$, -.323, and -1, and measured dispersions for the intermediate case.

Pulsed Quadrupoles

The pulsed quadrupole magnet design represents a compromise between several competing factors, i.e, it achieves an integral gradient of 5 kG and satisfies the aperture and length restraints imposed by the Booster lattice. Additional constraints were imposed on the magnet by the magnetic field rise time, field accuracy, and the desirability of powering the distributed magnets with a common power supply. A common power supply simplifies current matching in the magnets but dictates a magnet and transmission line design that minimizes the series inductance of the power circuit.

The quadrupole cross section is shown in figure 4. The external iron collar reduces the required current by approximately a factor of 2 relative to a similar air core magnet. It also serves as a rigid support for the magnet conductors and as a precision reference for conductor alignment and magnetic measurement. The collars were assembled with laminations stamped out of .025" AISI 1005 steel with a resistive coating to reduce eddy current effects.

The .25" square solid copper conductors are positioned in a grooved phenolic cylinder that provides electrical isolation and precisely locates the conductors. Cooling is completely passive via conduction through the phenolic and the collar. The 10 degree conductor placement angle ideally eliminates all field harmonics up to the 20-pole during constant field operation. During the 100 μs rise time, a small 12-pole field component is present due to eddy currents in the solid copper conductor. Undesireable field components due to the end connections were reduced by maintaining quadrupole symmetry in the end turns, by the use of welded joints to obtain precise radial conductor placement, and through field cancellation of the end fields from opposite ends

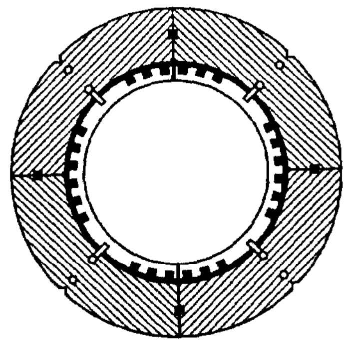

Figure 4. Pulsed Quadrupole Cross Section

of the magnet. Additional magnet parameters are listed in table 1.

TABLE 1.
Pulsed Defocusing Quadrupole Parameters

Gradient G/in @ 2 kA	480.
Magnetic Length in	9.7
Physical Length in	10.0
Physical Aperture in	6.0
Turns/pole	3
Inductance μH	18.0
Resistance mΩ	4.7

Power Supply

The power supply for the γ_t system is shown in Figure 5. The pulser consists of a single power supply connected to two parallel strings of six magnets each. Magnets in each loop are alternating F and D quadrupoles. A resonant charging scheme is used to double the rectifier voltage and to limit losses in the charging section. The discharge section is also a resonant LC circuit but with a freewheeling diode across the load. The load inductance and power supply capacitor form a resonant network at 2.5 kHZ to provide the 100 μs 1/4-sine-wave rise time. The diode clamps the capacitor voltage near zero at peak current and provides a current path for the L/R decay of the magnet current.

A balanced, shielded, stripline transmission line connects the power supply to the magnets and was designed to minimize its contribution to the system inductance while maintaining the proper resistance to give the desired decay time constant. The power supply output is balanced with respect to ground to keep the voltage to ground on the magnets less than 4 kV. The system is capable of charging the capacitor to 8 kV in 15 ms. At present, the capacitor voltage regulation is done open loop. If necessary, a closed loop system connected to the SCR phase controller can be implemented or a Q damping scheme for the charging chokes can be added to terminate the charging pulse. The power supply can deliver a 3300 A peak current

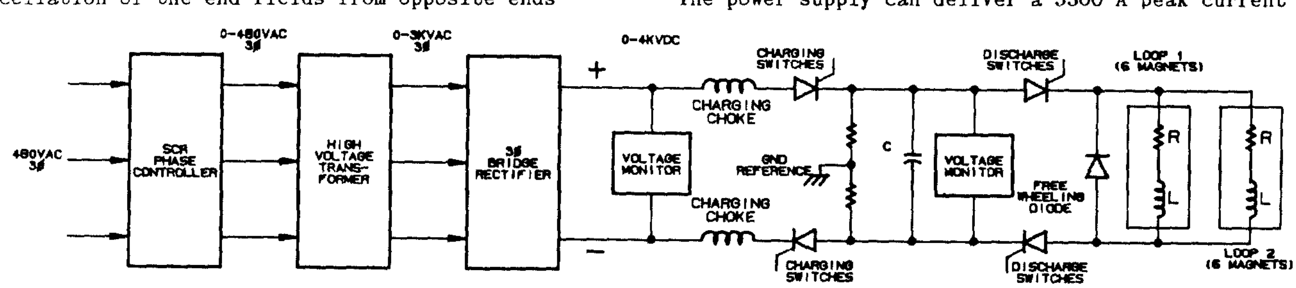

Figure 5. Power Supply and Circuit

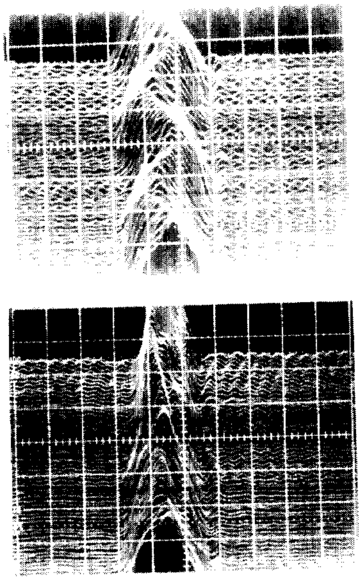

Figure 6. "Mountain range" pictures of a bunch passing through transition (below) and 5 msec later (above), with $\Delta\gamma_t$=-.75

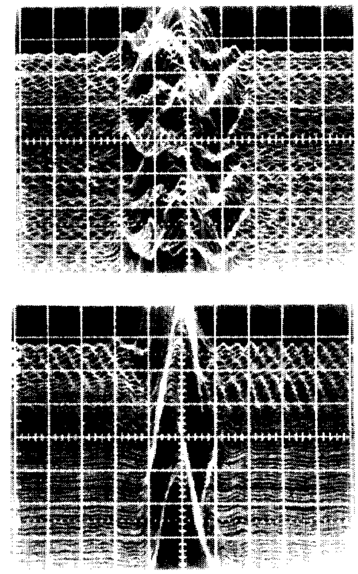

Figure 7. "Mountain range" pictures of a bunch passing through transition (below) and 5 msec later (above), without a transition jump.

pulse with 8 kV on the capacitor at a 15 Hz repetition rate. The current balance between the two loops is within 0.3%. Provisions are made in the power supply to trim the load impedances to improve this if necessary. The impedance of each loop is approximately 140 μH and 66 mΩ. Both charge and discharge switches are sets of series connected SCR's.

Longitudinal Matching

Longitudinal matching across transition can be optimized by varying the time of the transition jump. Matching requires that V'/η be the same before and after transition, where $\eta = \gamma^{-2} - \gamma_t^{-2}$ and V' is the slope of the effective ring voltage at the bunch. The contribution of space-charge effects to V' changes sign at transition; this effect can be compensated by changing the transition-jump timing.[5] In practice, timing is optimized by minimizing bunch length oscillations, which are easily observed on a peak-detected longitudinal pickup.

The dependence of the synchrotron frequency on γ_t has been exploited to measure the effect of the transition-jump system on γ_t. For this purpose, the frequency of the bunch length oscillations induced by deliberately mistiming the jump was measured. The results agree well with the SYNCH prediction. (This experiment was performed by S. Stahl and S. Holmes.)

Effects on Beam Dynamics

The "mountain range" pictures of Figures 6 and 7 show the evolution of a bunch with and without a transition jump of -.75 units, respectively. The intensity is about 1.5×10^{10} protons per bunch. Each picture shows 63 oscilloscope traces taken at 10-turn intervals, thus covering a total time of about 1 msec; successive traces are displaced upwards. The bandwidth of the pickup-cable-oscilloscope combination is about 1 GHz. The horizontal scale is 1 nsec/div. The lower picture in each figure shows the bunch passing thru transition, which occurs about halfway up each picture. The bunch gets somewhat shorter at transition, and the peak current somewhat greater, without the transition jump. The upper picture in each case shows a bunch about 5 msec after transition. The microstructure apparent on the bunch shape without the transition jump has been suppressed by the transition jump.

No perceptible losses were induced by the transition-jump pulse until the jump amplitude reached about a unit, at which point the losses were typically about 1%. The measured rms orbit displacement is .7 mm horizontally and .21 mm vertically for $\Delta\gamma_t$=-0.323 . Strong, predominantly dipole coupled-bunch instabilities in the latter half of the acceleration cycle constitute the major remaining problem affecting the evolution of the Booster beam in longitudinal phase space. The reduction of longitudinal emittance resulting from the transition jump unfortunately exacerbates these coupled-bunch effects. Thus it is likely that the benefits of the transition-jump system will be apparent in the output emittance only when the efforts presently underway to suppress the coupled bunch instabilities are completed.

Acknowledgments

The cooperation and support of our colleagues at Fermilab in the Booster group and in the Accelerator Division are gratefully acknowledged.

References

[1] W. Hardt, H. Schonauer, and A. Sorenssen, "Passing Transition in the Future CPS", in Proceedings of the Eighth International Conference on High-Energy Accelerators, 1971, pp. 323-326.

[2] A. Sorenssen, "Crossing the Phase Transition in Strong-focusing Proton Synchrotrons", Particle Accelerators 6, pp. 141-165, 1975.

[3] L. C. Teng, "Compensation of Space-charge Mismatch at Transition of Booster Using the Transition-jump Method",FNAL Phys. Note FN-207,April 17,1970.

[4] P. Lucas and J. MacLachlan, "Simulation of Space Charge Effects and Transition Crossing in the Fermilab Booster", submitted to this conference.

[5] K. Y. Ng, "Space Charge Effects of Transition Crossing in the Fermilab Booster", submitted to this conference.